An improved automated PQD classification method for distributed generators with hybrid SVM-based approach using un-decimated wavelet transform

An improved automated PQD classification method for distributed generators with hybrid SVM-based approach using un-decimated wavelet transform

Alper Yılmaz [a], Ahmet Küçüker [b], G okay Bayrak [a], Davut Ertekin [a,*], Miadreza Shafie-Khah [c], Josep M. Guerrero [d]

[a] Bursa Technical University, Faculty of Engineering and Natural Sciences, Department of Electrical and Electronics Engineering, 16300 Bursa, Turkey
[b] Sakarya University, Faculty of Engineering, Department of Electrical and Electronics Engineering, 54187 Sakarya, Turkey
[c] School of Technology and Innovations, University of Vaasa, Vaasa, Finland
[d] Center for Research on Microgrids (CROM), Department of Energy Technology, Aalborg University, 9220 Aalborg East, Denmark

A B S T R A C T

Artificial intelligence (AI) approaches are usually coupled with the wavelet transform (WT) for feature extraction to classify the power quality disturbances (PQDs). Therefore, selecting a useful WT-based signal processing approach is required for a reliable classification, especially in real-time applications. In this study, a new hybrid, un-decimated wavelet-transform (UWT)-based feature extraction method using a support vector machine (SVM) with a "á trous" algorithm is proposed to classify PQDs in distributed generators (DGs). The proposed method was performed in a real-time application of a DG system to classify PQDs. The derived features were tested on five different machine learning (ML) models by determining the most appropriate classification technique for the proposed UWT-based feature extraction method. An experimental DG system is constituted in the laboratory using a LabVIEW environment, and the proposed method is tested under different grid conditions. Besides, other well-known and studied conventional ML methods were also tested under 25 dB, 30 dB, and 40 dB noise and compared to the developed method. The experimental and simulation results show that the features extracted with the proposed UWT-based method provide much more successful results in classification than the existing wavelet methods in the literature. Furthermore, the proposed method's noise sensitivity performance is much better than other conventional wavelet algorithms, especially in real-time applications.

Keywords:
Power quality disturbances
Un-decimated wavelet transform
Machine learning
Distributed generation

Abbreviations: **CB**, Circuit Breaker; **CWT**, Continuous Wavelet Transform; **DbN**, Daubechies-N; **DCNN**, Deep Convolutional Neural Network; **DFIG**, Double-fed Induction Generator; **DGs**, Distributed Generators; **DT**, Decision Tree; **DWT**, Discrete Wavelet Transform; **EWT**, Empirical Wavelet Transform; **FT**, Fourier Transform; **GBDT**, Gradient Boosting Decision Tree; **kNN**, K-Nearest Neighbors; **ML**, Machine Learning; **PCC**, Point of Common Coupling; **pu**, Per-unit; **PQ**, Power Quality; **PQD**, Power Quality Disturbances; **RF**, Random Forest; **SNR**, Signal-to-noise Ratio; **ST**, S-transform; **STFT**, Short-Term Fourier Transform; **SVM**, Support Vector Machine; **UWT**, Un-Decimated Wavelet-Transform; **VMD**, Variational Mode Decomposition; **WPT**, Wavelet Packet Transform; **WT**, Wavelet Transform; **WTS**, Wind Turbine System; **WVD**, Wigner-Ville Distribution.

* Corresponding author.

E-mail addresses: alper.yilmaz@btu.edu.tr (A. Yılmaz), kucuker@sakarya.edu.tr (A. Küçüker), gokay.bayrak@btu.edu.tr (G. Bayrak), davood.ghaderi@btu.edu.tr (D. Ertekin), miadreza.shafiekhah@uwasa.fi (M. Shafie-Khah), joz@et.aau.dk (J.M. Guerrero).

1. Introduction

Power Quality (PQ) detection in the real-time domain is required for distributed generators (DGs) [1]. Continuous monitoring of PQ and detecting power quality disturbances (PQDs) ensures that the correct operating mode decision is made and allows components such as transformers, converters, and control equipment in the power system to operate with more reliability and with a longer life [2]. Besides, PQ parameters are essential factors in determining electricity usage cost, both in terms of production and regulation and consumption [3]. As a result, PQDs in the power system needs to be fast and accurately detected, and classified to improve PQ.

DG structure is an essential part of the microgrids [4]. The PQ problems occurring in the DG side with the integration of renewable energy systems show similar features to conventional systems. However, PQDs in micro-grid applications are more complex to identify than conventional power systems. As with conventional systems, short circuit faults, switching of large loads, switching large capacitor banks, drive systems with nonlinear loads, and transformers energization will lead to transients, sudden current/voltage drops and rises, and voltage fluctuations, harmonics, etc. in the micro-grid. On the other hand, some situations cause PQDs specific to DGs, such as enabling or disabling DGs, presence of nonlinear loads, inverter control strategies, and operating mode switching (islanding/non-islanding) [5]. In addition, environmental characteristics such as variation in solar radiation and wind speed are also effective in the degradation of PQ in renewable energy-based DG systems [3,6]. If the PQDs are distinctly classified and known in advance in DG-based systems, an appropriate mitigation approach can be adopted and thereby enhance the performance of the power electronic equipment and control devices. Therefore, effective operation, control, and protection of the DG system from unwanted operations are possible by detecting and classifying PQDs with a suitable method.

Today, the PQ analyzers use the effective value conversion method to detect and classify the short-and long-term voltage distortions. Although these methods can be applied easily, they have many disadvantages, such as difficulty, threshold values selection, uncertainty caused by operating conditions, involving undetected areas, and being easily affected by noise [2]. Many of the signal processing-based and artificial intelligence-based methods related to PQD detection and classification have been proposed in recent years, differing from conventional power analyzer methods to eliminate these disadvantages [3]. Besides, signal processing-based methods use both time and frequency components of a signal, unlike other methods. Therefore, it is more flexible and reliable in comparison with the conventional PQD detection and classification methods.

The proposed signal analysis methods for PQD detection and classification in literature can be grouped as Fourier Transform (FT) and its variances, wavelet transform (WT) and its variances, variational mode decomposition (VMD), s-transform (ST), Hilbert-Huang transform, and Wigner-Ville Distribution (WVD). FT methods do not allow the local inspection of frequency components. It cannot give a proper spectrum in non-stationary signals (transients, short-term voltage sag/swell, etc.). This problem was solved by the windowing process used in the short-term Fourier transform (STFT). STFT has a fixed window size and is not suitable for simultaneously examining the signal's high and low-frequency components [7]. ST does not satisfy the real-time requirements for PQD detection since it is based on block processing. Decomposition of the signals using Hilbert-Huang transform with close frequency components and during sudden transition such as PQDs is difficult [2]. The most important resulting limitations of the VMD method are the boundary effects and sudden signal onset in general. WT-based methods have flexible time–frequency representation. WT methods can detect signal discontinuities and sudden changes in high-grade derivatives where other signal processing methods cannot detect. However, WT methods perform low performance under noise. The most commonly used WT-based methods for the detection and classification of PQDs can be examined in 3 groups as continuous wavelet transform (CWT), discrete wavelet transform (DWT), and wavelet packet transform (WPT) [8–13].

The performances of WT techniques for PQD detection and classification are shown in Table 1. DWT, CWT, and WPT methods are used for PQD detection and classification, but these methods have some drawbacks and limitations in the classification of PQDs. In this study, unlike the conventional techniques, the un-decimated wavelet transform (UWT) method, which is mostly used in image processing, was used. It has not been used in the power system already as the feature extraction in the classification of PQDs. In ref. [14], the UWT method is suggested for fault detection in PV-based microgrids for the first time. This method has been tested in real-time applications, and it overcomes the drawbacks and limitations of WT methods. UWT reduces the oscillations and noise in the measured voltage quantities. UWT is useful for selecting threshold values rather than DWT, and noise sensitivity is lower than other WT-based applications [15].

Various artificial intelligence-based algorithms have been used in the literature to classify PQDs in DG applications. AI-based detection and classification methods for PQDs constituted of neural network-based classifiers [16,17], support vector machine (SVM)-based classifiers [18,19], fuzzy expert system-based classifiers, decision tree (DT), random forest (RF) classifiers, and deep learning-based classifiers [3]. These methods, which have superiority over other methods are classified with multiple classifiers along with powerful features are extracted over the original signal with the appropriate signal processing method. An important aspect of feature extraction is signal analysis. In this study, a new UWT-based signal analysis method with a "á trous" algorithm is proposed to feature extraction of PQDs. To assess the performance of the proposed scheme, different classifiers have been considered. The overall recognition test accuracy for the PQDs is 99.85% for the proposed UWT and kernel SVM-based hybrid method. The classification accuracy under low-level noise and high-level noise conditions is 99.66% and 99.32%, respectively.

The Contribution of the Study can be summarized in three sections:

- To improve the resolution of time–frequency analysis, an UWT-based decomposition method with a "á trous" algorithm was used for the first time in the classification of PQDs among the existing WT-based methods. The improved UWT method has advantages in noise reduction, peak or valley detection and it obtains high-frequency resolution at high frequencies.
- The performances of five different classifiers on the most used WT and proposed UWT methods were examined in detail. The classifiers' performance, which is developed based on WT but has dramatically low performance under noise, has been improved with UWT.

Table 1
Performances of WT-based methods for PQD detection and classification.

	DWT	CWT	WPT	UWT
Peak Detection Accuracy	Not Robust	—	Robust	**Robust**
Real-Time Fault Detection	Most Suitable	Not Suitable	Suitable	**Suitable**
Prevalence of use	High	Low	Moderate	**New**
Response Time	**Very short**	Long	Short	Short
Noise sensitivity	High	Moderate	High	**Very Low**
Non-stationary analysis	Suitable	Suitable	Suitable	**Most suitable**
Feature extraction process	Not suitable for noisy conditions	Not suitable for real-time	Not suitable for noisy conditions	**Most suitable**

- The UWT and SVM-based hybrid method was performed with high accuracy and reliability even under noise from 25 to 40 dBs.

This paper is structured into five sections. Section 2 presents synthetic PQD generation, details of the UWT decomposition, parameter design, and feature extraction process. At the same time, UWT advantages are presented in detail in this section. The proposed methodology for the classification of PQDs is investigated in Section 3. Section 4 covers mathematical, simulation, and real data results related to the classification of PQDs. In addition, a comparative analysis of the proposed method with existing methods is given in this section. Finally, Section 5 concludes the proposed research work details.

2. Methodology

The graphical abstract of this paper is given in Fig. 1. In the first stage, PQD data were generated from both the integral-based mathematical method in the LabVIEW environment and the simulations performed using the modeled micro-grid in MATLAB. Different levels of noise were added to the generated PQDs and these signals were preprocessed. Then, an UWT-based decomposition with the "á trous" algorithm was applied to the event signals and different levels of detail coefficients were obtained. After the decomposition, feature vectors for nine classes were determined. The feature vector is the input to the improved kernel SVM. At the output of the SVM classifier, there are PQD event output labels (C1, C2, …, C9). When the SVM model was created, the validity of the proposed method is tested with the PQD data acquired by using the experimental test system.

2.1. PQD data generation

Most of the available literature used a mathematical model or simulation model for the generation of data due to the difficulty of obtaining the real signals related to the PQD. In this study, the integral-based mathematical model was used to produce PQD signals [20]. The most common PQD signals, especially in microgrid applications, were provided automatically in the LabVIEW environment according to the IEEE standards [21]. Besides, different levels of noise can be applied to generated PQD signals through the program interface.

Different parameters for the PQD signals can be presented as bellows:

- The fundamental frequency value is 50 Hz.
- The sampling frequency is 10 kHz.
- The number of cycles of the fundamental frequency is ten cycles (0.2 s-2000 points).
- The number of samples for each class is 2000.
- The amplitude of the PQD signals is based on per-unit (pu)

Many studies have been examined [20–26] to obtain the mathematical model for the eight most common PQD events in the power system. Table 2 shows that training, validation, and test dataset can be generated randomly by the software created based on the equations specified among the possible PQD parameter values. Additionally, unlike other studies, voltage drops/rises, the frequency drops/increase, signals containing low harmonics, and their multiple states can be obtained with the proposed software using LabVIEW in nominal signal generation under normal conditions within the limits of IEEE standards. The variety in the nominal signal data has increased system flexibility and reliability. Waveforms and definitions of the most common PQDs specified in IEEE 1159 std [22].

To simulate the PQDs in a noisy environment, the ideal PQD waveforms with White-Gaussian noise have been considered. The definition of signal-to-noise ratio (SNR) can be expressed as

$$SNR = 10log_{10}\left(\frac{P_s}{P_n}\right)dB \tag{1}$$

where P_s and P_n refer to the average power of the ideal signal and noise signals, respectively. The database of PQDs for SNR=∞, SNR = 40 dB, SNR = 30 dB, and SNR = 25 dB.

2.2. Un-decimated wavelet transform (UWT)

The WT, which is often used in pattern recognition applications, can decompose signals at different scales and resolutions. WT-based DG

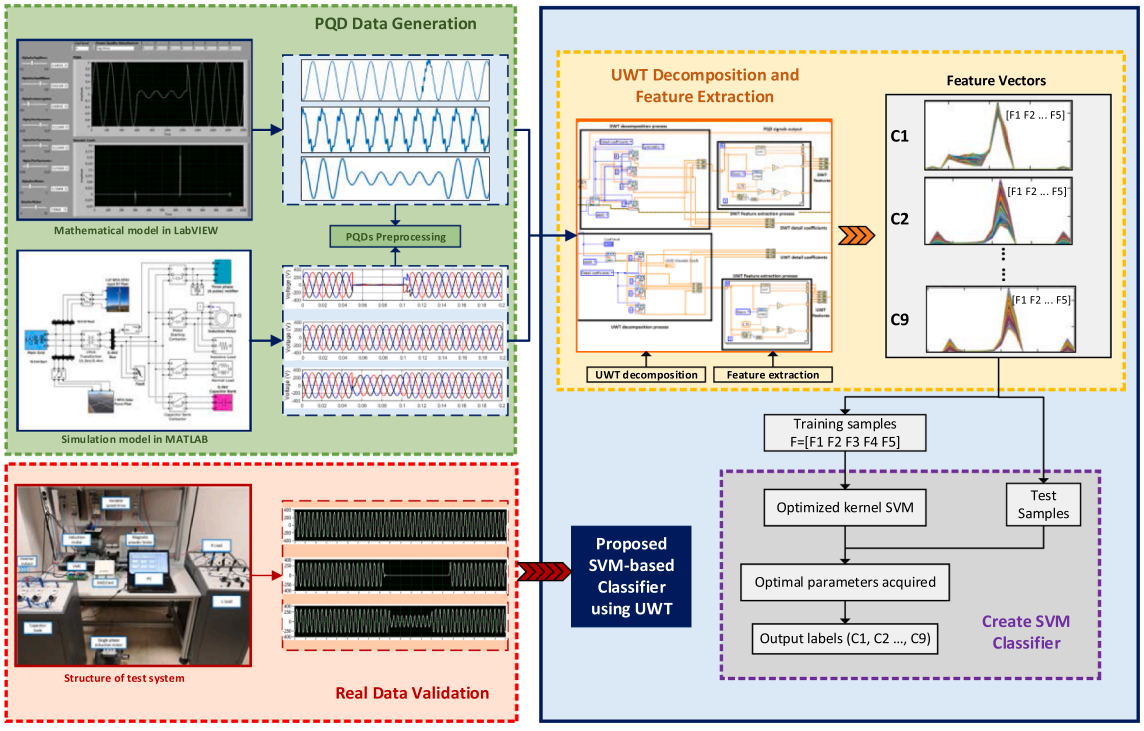

Fig. 1. Graphical abstract of this paper.

Table 2
Mathematical model of PQDs [20–26].

Class	PQD Signals	Equations	Threshold Parameters
C1	Nominal	$x(t) = \sin(2\pi ft-\varphi)x(t) = [1-\alpha(u(t-t_1)-u(t-t_2))]\sin(2\pi ft-\varphi)x(t) = [1+\beta(u(t-t_1)-u(t-t_2))]\sin(2\pi ft-\varphi)x(t) = \sin(2\pi ft-\varphi)+\sum_{n=3}^{7}\alpha_n\sin(2\pi f_i t-\varphi_i)$	$49.8\le f\le 50.2,\ -\pi\le\varphi\le\pi$ $0\le\alpha<0.1,\ 0\le\beta<0.1$ $u(t)=\begin{cases}0, t<0\\1, t\ge 0\end{cases}\ \alpha_n<0.03$
C2	Sag	$x(t) = [1-\alpha(u(t-t_1)-u(t-t_2))]\sin(2\pi ft-\varphi)$	$T\le t_2-t_1\le 9T$ $0.1\le\alpha<0.9$
C3	Swell	$x(t) = [1+\beta(u(t-t_1)-u(t-t_2))]\sin(2\pi ft-\varphi)$	$T\le t_2-t_1\le 9T$ $0.1\le\beta<0.8$
C4	Interruption	$x(t) = [1-\gamma(u(t-t_1)-u(t-t_2))]\sin(2\pi ft-\varphi)$	$T\le t_2-t_1\le 9T$ $0.9\le\gamma<1$
C5	Harmonics	$x(t) = \sin(2\pi ft-\varphi)+\sum_{n=3}^{7}\alpha_n\sin(n\pi ft-\vartheta_n)$	$n=\{3,5,7\};\ 0.05\le\alpha_n\le 0.15$ $-\pi\le\vartheta_n,\vartheta_n',\vartheta_n''\le\pi n'=\{3,5,7\};$ $0.05\le\alpha_{n'}\le 0.15$ $n''=\{1,3,5\};$ $\alpha_{n'}=1 \mid n''=1; 0.05\le\alpha_{n'}\le 0.15 \mid n''=\{3,5\}$
C6	Flicker	$x(t) = [1+\delta\sin(2\pi f_i t)]\sin(2\pi ft-\varphi)$	$0.05\le\delta<0.1$ $8\le f_i<25$ Hz
C7	Oscillatory transient	$x(t) = \sin(2\pi ft-\varphi)+\beta\exp(-(t-t_1)/\tau\sin(2\pi f_n(t-t_1)-\vartheta)((u(t-t_2)-(u(t-t_l))$	$300Hz\le f_n\le 900Hz;$ $8\text{ms}\le\tau\le 40ms;\ -\pi\le\vartheta\le\pi 0.5$ $T\le t_2-t_1\le 3T$
C8	Impulsive transient Spike	$x(t) = \sin(2\pi ft-\varphi)+\sigma(\exp(-750(t-t_a)-\exp(-344(t-t_a))((u(t-t_a)-u(t-t_b)))$	$0.222\le\sigma<1.11;$ $T\le t_a\le 9T$ $t_b=t_a+1ms$
C9	Notch	$x(t) = \sin(2\pi ft-\varphi)-sign(\sin(2\pi ft-\varphi))+\sum_{n=0}^{10c-1}\alpha_n\sin(n\pi ft-\vartheta_n)k(u(t-(t_c+s.n)-u(t-(t_d+s.n)))$	$0.01\ T\le t_d-t_c\le 0.05T;$ $t_d\le s; t_c\ge 0;$ $0.1\le k<0.4$ $c=\{1,2,4,6\}; s=\frac{T}{c}$

systems methods can be examined under four headings: the CWT, DWT, WPT, and UWT. WT uses the mother wavelet (ψ(x)) function as a scalable window concept instead of the windowing concept used in the STFT. The CWT is using parameter b is the shifting factor, and the scaling factor is s. The CW function ($\psi_{s,b}$) is expressed as in equation (2). CWT is determined through equation (3) by using the wavelet function [27].

$$\psi_{s,b}=\frac{1}{\sqrt{s}}\psi\left(\frac{t-b}{s}\right) \tag{2}$$

$$CWT(s,b)=\frac{1}{\sqrt{s}}\int_{-\infty}^{\infty}f(t)\psi\left(\frac{t-b}{s}\right)dt \tag{3}$$

CWT method is done through a limited real-time process because of the intensive computation. DWT is designed by using filter banks to remove the disadvantage of the computational load in the CWT. The DWT performed to signal as equation (4) using $g_{j,k}(n)$ main wavelet function (equation (5)).

$$DWT(j,k)=\sum_{n\in Z}\sum_{k\in Z}S(n)g_{j,k}(n), g_{j,k}\in Z, j\in N, k\in Z \tag{4}$$

$$g_{j,k}(n)=a_0^{\frac{-j}{2}}g\left(a_0^{j}n-kb_0\right) \tag{5}$$

The relation between S(n) and $g_{j,k}$ (n) can be expressed as

$$S(n)=\sum_{n\in Z}\sum_{k\in Z}d_{j,k}g_{j,k}(n) \tag{6}$$

As a result of the decomposition performed with DWT, approximation coefficients (cA_n) and detail coefficients (cD_n) are obtained. Wavelet coefficients can be calculated by

$$cA[n]=\sum_{k}S(k)g[2n-k]; cD[n]=\sum_{k}S(k)h[2n-k] \tag{7}$$

The UWT method uses filter banks like DWT, but the coefficients' length is the same as the main signal [14]. Detail and approximation coefficients are up-sampled using multi-resolution analysis by the "á trous" algorithm in the UWT method [27]. UWT can reduce oscillations and noise, and it is useful for selecting the threshold values rather than DWT [15]. UWT detail and approach coefficients can be expressed as

$$c_j^U[k]=\left(h_0^{(j)}*c_{j-1}^U[k]\right)=\sum_n c_{j-1}^U\left[k+2^j n\right]h_0(k)\big];$$

$$w_j^U[k]=\left(h_0^{(j)}*c_{j-1}^U[k]\right)=\sum_n c_{j-1}^U\left[k+2^j n\right]h_1(k)\big] \tag{8}$$

2.2.1. UWT advantages

Compared to other WT methods, the UWT method has advantages in noise reduction, peak or valley detection, and real-time signal analysis [28]. Fig. 2.a. shows the UWT and DWT-based denoising methods results for a voltage sag signal. In the performed analysis using the Wavelet Denoise Express VI block [29], 8-level decomposition was implemented using the db4 wavelet. As a result of the UWT-based noise-reduction process, a more successful result was achieved compared to the DWT-based method. In addition to requiring some processing load, a more successful result was achieved as a result of the UWT-based noise reduction process than the DWT-based method. In Fig. 2.b., the accuracy of the UWT-based and DWT-based peak/valley detection methods is examined for the transient signal. Threshold values are 1 pu for the peak and set to 0 pu for the valley. It is seen that the detection process with UWT is more reliable compared to the DWT-based method. The reason for this is that the UWT-based method at the first stage finds the zero-crossing point in low-resolution signals and then applies the same process to the higher resolution coefficients. Detection of zero crossings reduces the noise when is applied to the low-resolution coefficients and increases the sensitivity of the detecting positions with the highest amplitude when applied to the high-resolution coefficients.

2.2.2. Mother wavelet selection

In WT applications, the selection of a proper mother wavelet plays an important role in detecting analysis various types of PQDs. PQD signals

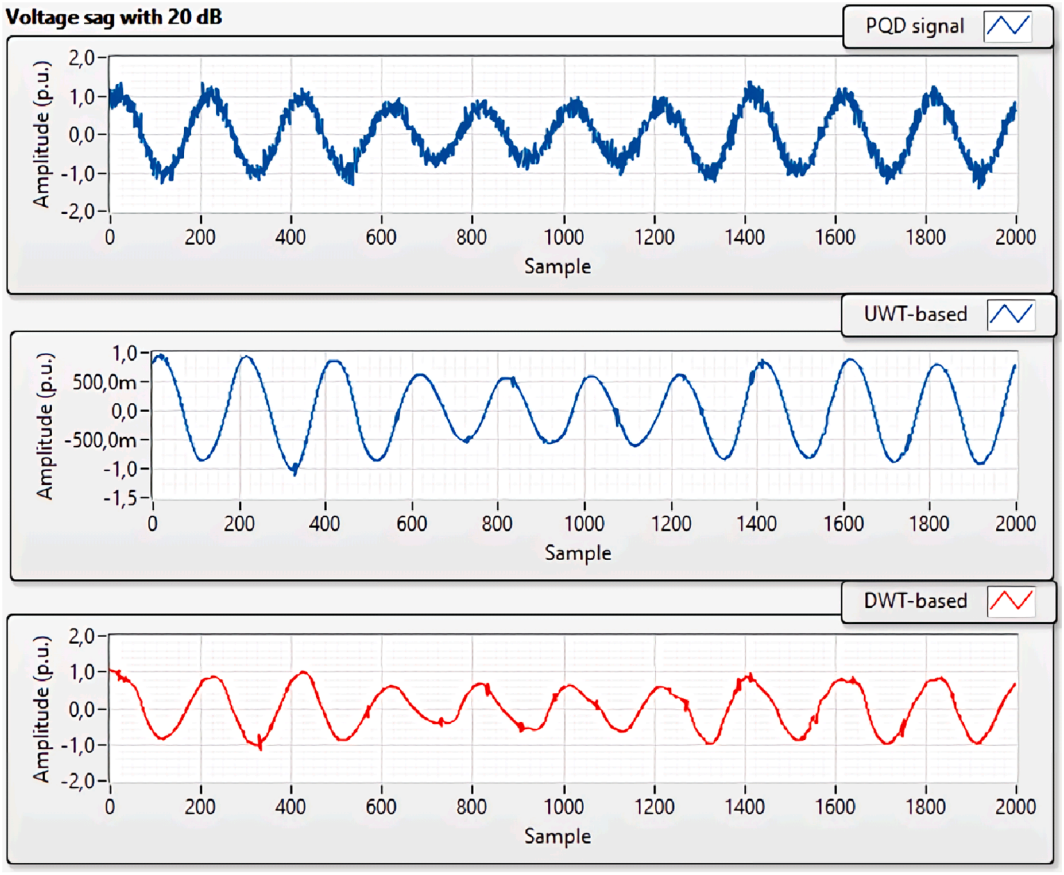

(a)

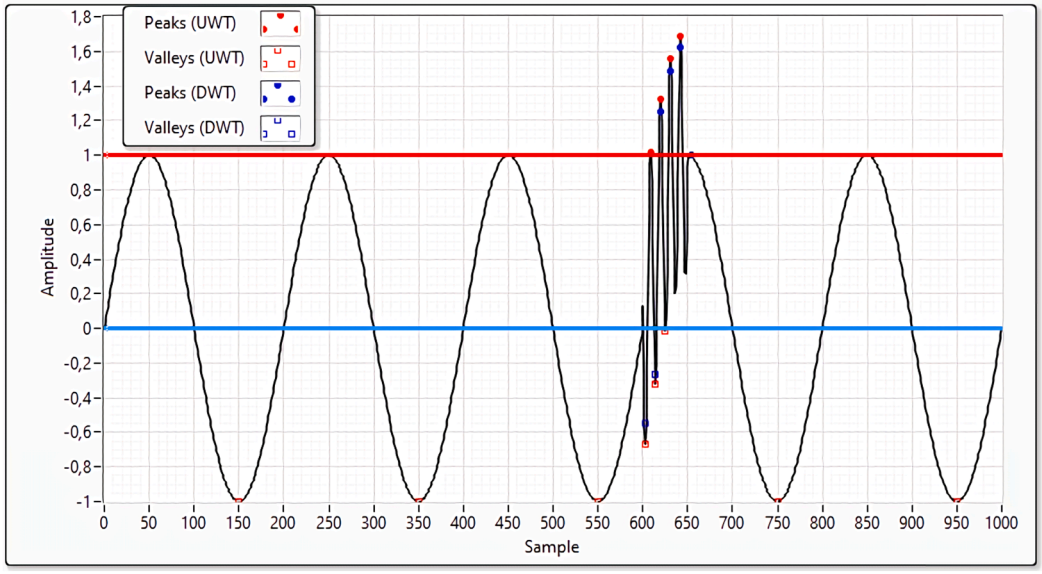

(b)

Fig. 2. **(a)** Comparison of methods for WT-based noise reduction, and **(b)** peak-valley detection.

have a high-frequency component for short time durations. Daubechies (dbN) wavelet family is the most useful wavelet type for PQD detection and classification. While selecting the mother wavelet for PQD classification, it is essential to provide a better time location at low scales. The mother wavelet type used in PQD detection is "dbN" wavelets in different studies like [2,9,14,30]. In this study, different simulation and experimental tests were performed to define the wavelet type. The db4 mother wavelet has been selected in the study. The computational time is reduced using the db4 mother wavelet containing a short wavelet type with a few samples [17]. The reason for the db4 selecting is that it is the

most localized, i.e. compactly supported, in time. The computational time of the 2-level UWT decomposition and UWT get coefficients stage with different dbN wavelets was measured using the subprogram given in Fig. 3. For this process that has been performed on the recorded data, the determined computational times are given in Table 3 for different wavelet types. The calculation time of the db4 wavelet is suitable for system performance.

2.2.3. *Decomposition level selection*

The conducted studies show that 8-level decomposition is sufficient for PQD classification for DWT and UWT-based signal analysis methods. The frequency ranges of the detail and approximation coefficient components for 8-level decomposition are shown in Table 4. As a result of the analysis, the frequency range in which events such as voltage drop/rise are prominent corresponds to the low-frequency bands (d5, d6, d7). On the other hand, disturbances such as transient events with a high-frequency component can be observed in analysis in the high-frequency range (d2, d3, d4).

2.3. *Feature extraction*

The most common statistical parameters have been obtained from the literature that is used for feature extraction. While features with high complexity and processing load are used in the literature, in this study, simple features of the detail coefficients obtained after UWT decomposition are used in the classifier input. Fig. 4 shows the developed block diagram for UWT decomposition and feature extraction. In subprogram 1, noise addition and 8-level UWT analysis are applied to PQD events, and feature extraction is performed in subprogram 2.

In Fig. 5, the general structure of the feature extraction method is given. The feature extraction process starts with UWT decomposition with "á trous" algorithm applied to the PQD signals generated using the Integral-based mathematical model. The detail coefficients are determined using the "db4" mother wavelet for 8-level decomposition After the decomposition process, the mean (μ), standard deviation (σ^2), variance (σ), entropy (E), and energy (E_j) values of the obtained detail coefficients (D_1, D_2, D_3 … D_8) are calculated. Features are normalized using the min–max normalization technique. The feature vectors are given by

$$F1 = [\mu_{D1}\mu_{D2}\mu_{D3}\mu_{D4}\cdots\mu_{D8}]$$

$$F2 = [\sigma^2{}_{D1}\sigma^2{}_{D2}\sigma^2{}_{D3}\sigma^2{}_{D4}\cdots\mu\sigma^2{}_{D8}]$$

$$F3 = [\sigma_{D1}\sigma_{D2}\sigma_{D3}\sigma_{D4}\cdots\sigma_{D8}]$$

$$F4 = [En_{D1}En_{D2}En_{D3}En_{D4}\cdots En_{D8}]$$

$$F5 = [E_{D1}E_{D2}E_{D3}E_{D4}\cdots E_{D8}] \quad (9)$$

After normalization of the data, the feature vector is given as

Table 3
Computing time for different wavelet types.

Wavelet Type	Computational Time (s)	Wavelet Type	Computational Time (s)
db	—	db08	0.0134104
db02	0.0118995	db09	0.0141892
db03	0.0120056	db10	0.0147398
db04	**0.0123345**	db11	0.0151829
db05	0.0127549	db12	0.0158798
db06	0.0130931	db13	0.0164289
db07	0.0132104	db14	0.0169797

Table 4
The frequency ranges of the coefficients for 8-level decomposition.

Decomposition Level	Coefficient	Frequency range
1	Detail 1 (d1)	2,5–5 kHz
2	Detail 2 (d2)	1,25–2,5 kHz
3	Detail 3 (d3)	625 Hz-1,25 kHz
4	Detail 4 (d4)	312–625 Hz
5	Detail 5 (d5)	156–312 Hz
6	Detail 6 (d6)	78–156 Hz
7	Detail 7 (d7)	39–78 Hz
8	Detail 8 (d8)	0–39 Hz

$$F = [F1F2F3F4F5] \quad (10)$$

F1-Mean of coefficients: After calculating the UWT detail coefficients for eight levels, the mean of these coefficients is taken as a feature. The sub-program derives the mean value using equation (11).

$$\mu = \frac{1}{n}\sum_{i=0}^{n-1} x_i \quad (11)$$

where μ is mean, and n is the number of the elements in the coefficients at the specified decomposition level.

F2-Variance of coefficients: The variance gives information about the distribution of data. It is also expressed as the average distance of the values from the means. The sub-program calculates the difference using the equation (12).

$$\sigma^2 = \sum_{i=0}^{n-1}\frac{(x_i-\mu)^2}{w} \quad (12)$$

where σ^2 is variance, w is (n-1) when weighting is set to the sample.

F3-Standard deviation of coefficients: Standard deviation is a statistical measure that shows the spread of the most used data for the quantitative scale numbers in general. The sub-program calculates variance value using the equation (13).

$$\sigma = \sqrt{\sum_{i=0}^{n-1}\frac{(x_i-\mu)^2}{w}} \quad (13)$$

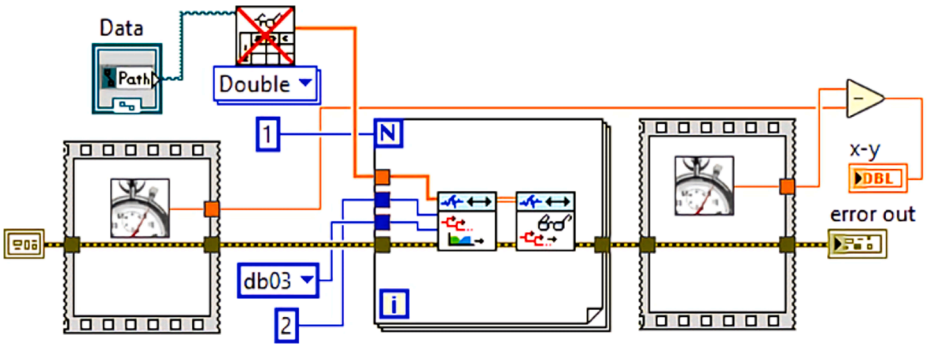

Fig. 3. Block diagram of the computing time for different wavelet types.

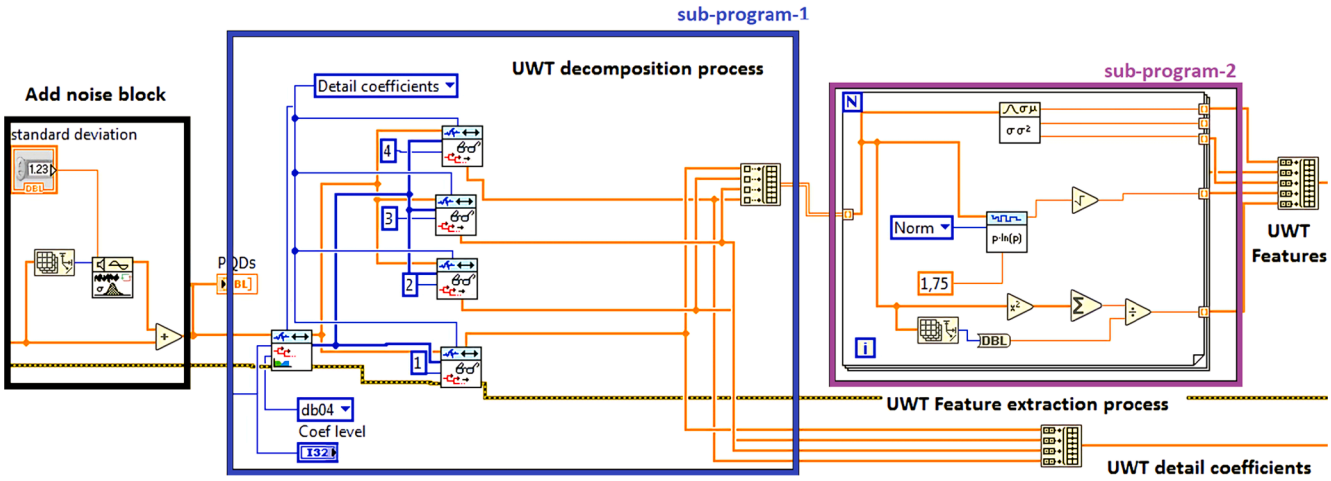

Fig. 4. Developed feature extraction process in LabVIEW.

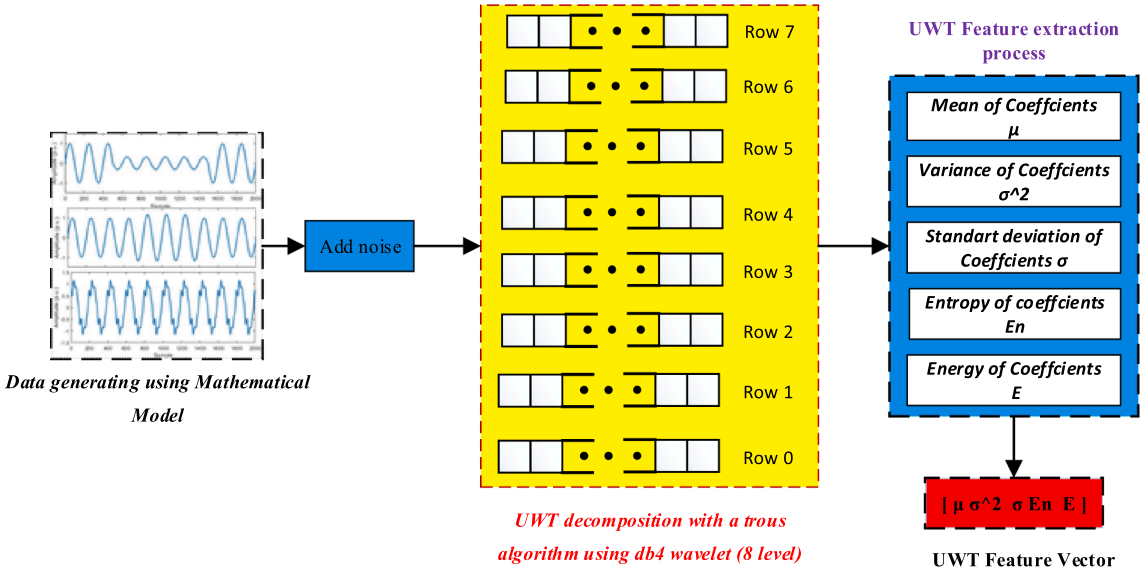

Fig. 5. The architecture of the proposed feature extraction process.

F4- Entropy of coefficients: Entropy, used in scientific studies, is a unit of measure that expresses the irregularity of the elements in the data set with real numbers. Although there are different entropy formulas, the Shannon Entropy law in information theory is usually expressed by equation (14) as a random variable:

$$En = -\sum_{j=1}^{N}\left\{D_{ij}^{2}\log(D_{ij}^{2})\right\} \tag{14}$$

where $i = 1, 2, \ldots, l$ represents the number of WT decompositions at level l, and N is the number of coefficients for each level.

F5- Energy of coefficients: The energy feature extraction technique is applied to UWT coefficients of the PQD signal. The coefficients' energy is found in equation (15) to represent the level of j: decomposition, d: detail coefficients, N: a number of detail coefficients.

$$E = \sum_{n=1}^{N}|D_{jn}|j = 1, \cdots\ldots, l \tag{15}$$

2.3.1. Feature analysis using UWT

To verify the effectiveness of the proposed UWT-based feature extraction method, UWT specifications are compared with DWT features for analyzing PQDs. Fig. 6 illustrates the comparison results of DWT and UWT standard deviation and entropy (F3, F4) features under noisy and noise-free conditions. The start and end time of the voltage sag event is 0.055 s (Sample 551) and 0.126 s (sample 1262). The amplitude of the voltage signal between these seconds decreased to 68.5% of the nominal value. Fig. 6 shows that UWT reduces the oscillations and noise in the F3 and F4. The features obtained as a result of the decomposition with DWT are significantly affected by the noise. Different features obtained under the noise will significantly reduce the performance of the classifier and make complex structures necessary. This indicates that the features obtained by UWT with "a trous" decomposition, overcomes the drawbacks and limitations of traditional WT-based methods.

2.4. Support vector machine (SVM)

SVM method purposes finding a separation hyperplane in the classes of the n-dimensional feature space. These hyperplanes can be achieved with a small number of support vectors. In this way, successful results can be obtained in training sets with a low number of data. The best hyperplane is obtained by determining the furthest to class members. SVM, which has achieved very successful results in solving linear problems, takes the data to a new dimension by making nonlinear

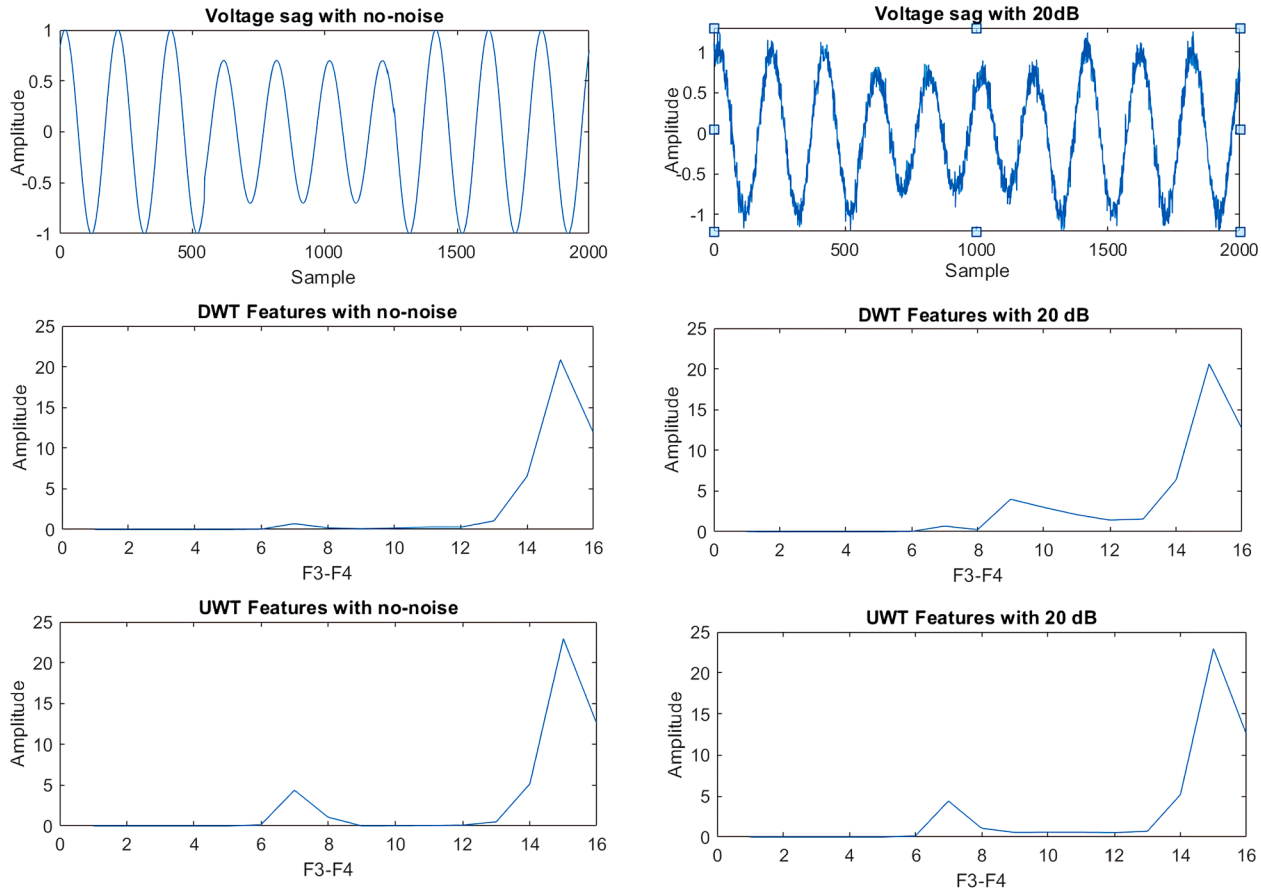

Fig. 6. Comparison results of DWT and UWT features for voltage sag event.

mapping through kernel functions in nonlinear problem solutions. The classification is carried out by determining the optimum separation hyperplane (OSH) in the new space. In this study, we used the SVC function of the Scikit ML library. For given training vectors $x_i \in R^p, i = 1, 2 \cdots .. n$, in two classes, and a vector $y \in \{1, -1\}^n$ SVC function solves the main problem given with equation (16).

$$min_{w,b,\zeta} \frac{1}{2} w^T w + C \sum_{i=1}^{n} \zeta_i \tag{16}$$

$$subjecttoy_i \left(w^T \phi(x_i) + b \right) \geq 1 - \zeta_i, \zeta_i \geq 0, \mathrm{i} = 1, 2, \cdots, \mathrm{n}$$

Its dual is

$$min_{\alpha} \frac{1}{2} \alpha^T Q \alpha - e^T \tag{17}$$

$$subjecttoy^T \alpha = 0, 0 \leq \alpha_i \leq C, i = 1, 2, \cdots, n$$

where e is the vector of all ones, Q is a positive semi defined matrix. When one uses kernel function, this matrix can be described as $Q_{ij} \equiv y_i y_j K(x_i, x_j)$ where the kernel function is presented by $K(x_i, x_j) = \phi(x_i)^T \phi(x_j)$. For training vectors, the function ϕ provides mapping into a higher (maybe infinite) dimensional space. The decision function can be expressed as

$$sgn\left(\sum_{i=1}^{n} y_i \alpha_i K(x_i, x) + \rho \right) \tag{18}$$

3. The proposed method based on hybrid UWT and SVM

In this study, a hybrid model that uses an SVM classifier with the UWT signal processing method was investigated for PQD classification. In the proposed method, UWT coefficients are obtained by an 8-level UWT decomposition after pre-processing signals acquired from the point of common coupling (PCC). The average, standard deviation, variance, entropy, and energy of each level coefficient are determined, and a feature dataset is created with these values calculated for all levels. Feature dataset applied to train the SVM and test them for performance assessments. Its flowchart is shown in Fig. 7.

The framework UWT-SVM can be divided into two parts: 1) UWT-based time–frequency analysis then feature extraction and 2) SVM-based automatic classification of PQDs.

For the application of equation (8) to the voltage signal where v_k is voltage sequence, UWT coefficients can be calculated through (19):

$$[cv_k]_j^U = \sum_n [cv]_{j-1}^U \left[k + 2^j n \right] h_0(k) \big];$$

$$[wv_k]_j^U = \sum_n [cv]_{j-1}^U \left[k + 2^j n \right] h_1(k) \big] \tag{19}$$

The features μ, σ^2, σ, *En*and, *E* are obtained from each level of detail coefficients. These features are obtained to compute the weighted linear combination kernel as in [31]. Then, the PQDs are classified by automatic SVM.

The conventional SVM method uses only one kernel function to map the features data. However, this situation decreases the performance rate in the classification of signals containing many different properties, such as PQDs. A weighted linear combination kernel is proposed in [31] to enhance the ability of the classification. The optimization framework of the SVM is described as

$$\min_{w,b,\xi_i} \left\{ \frac{\|w\|^2}{2} + C \sum_{i=1}^{n} \xi_i^2 \right\}$$

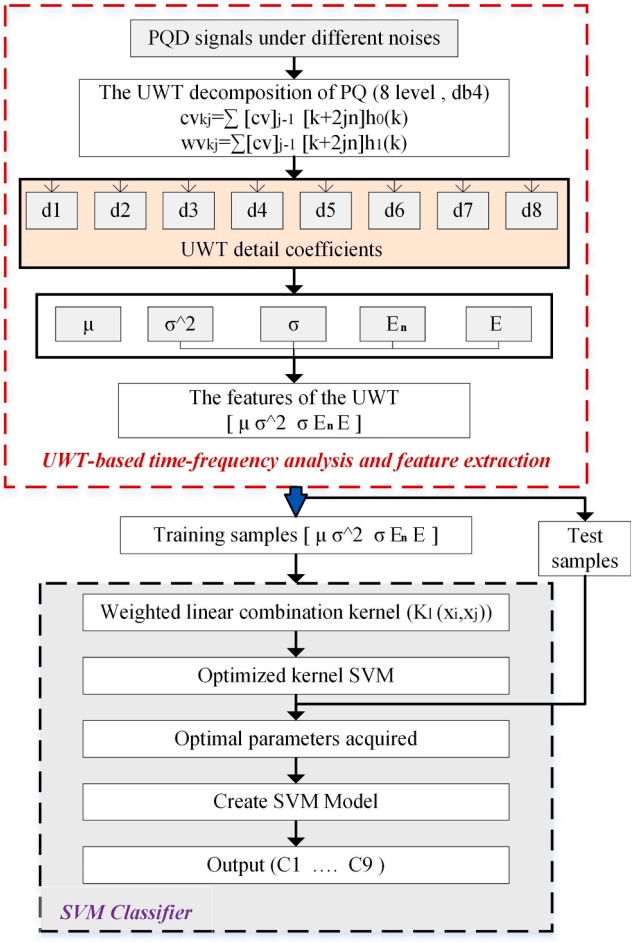

Fig. 7. The flowchart of the proposed UWT and SVM-based method.

$$s.t.y_i\left(w^T K_l\left(x_i,x_j\right)+b\right)\geq 1-\xi_i$$

$$\xi_i \geq 0, i=1,\cdots,n \tag{20}$$

where K_l denotes the weighted linear combination kernel for the two pointsx_i, x_j, w indicates the weight vector, b presents the bias, C denotes the penalty coefficient and, ξ_i illustrates slack variable. The decision function can be expressed as (18).

4. Experiments and evaluations

Experimental studies are performed under different conditions to verify the effectiveness of the proposed hybrid UWT-SVM method. The proposed hybrid method's performance is investigated by comparing it to different machine learning (ML) methods. The ML-based multiclass classification experiments conducted in this research were carried out using Google Colaboratory, Tesla P100 GPU with 12 GB RAM. We used Python programming language and Keras, a high-level neural network API built on the TensorFlow framework in Google Colaboratory. Scikit-Learn, Pandas, and Seaborn libraries are used for model implementation, data analysis, and data visualization, respectively.

The feature dataset was imported and shuffled. For splitting the dataset into training and test data, we used a 0,7 ratio. For every multiclass classifier, we did several experiments by changing the model parameters. The multiclass classifier model parameters, which give each model's best accuracy score, are presented in Table 5.

To select a proper kernel function, linear, polynomial, and Gaussian kernels are used to validate the SVM model. When the performances are examined, all functions of the combination kernel are selected as gaussian kernels because of their simplicity and higher accuracy. In the selection of the parameters of the kernel functions, an appropriate range of values is determined in the first step, by making use of previous experiences. In the second step, the optimal parameters are selected by the grid search method and specify the size of the kernel cache. After the kernel function and weight coefficients are selected, further researches are explored. Performance tests are performed for different kernel SVM parameters and the best parameters of the gaussian kernel (K_l) and penalty coefficient (C) is determined by using the grid search method.

Table 5
Multiclass classifier parameters.

Classifier	Parameter Set
kNN	n neighbors = 3, leaf size = 30, metric='minkowski', weights = uniform, p = 2.
SVM	**kernel = gaussian, cache size = 200, max iteration = 1, C = 200.0, step size = 0.01, K_l = 3, 2, tol = 0.001**
DT	criterion = gini, splitter = best, minimum samples split = 2, minimum samples leaf = 1, ccp alpha = 0.0 minimum weight fraction leaf = 0.0, presort='deprecated', minimum impurity decrease = 0.0
RF	criterion = gini, n estimators = 500, minimum samples split = 2, minimum samples leaf = 1, minimum weight fraction leaf = 0.0, minimum impurity decrease = 0.0, verbose = 0, ccp alpha = 0.0
GBDT	loss = deviance, learning rate = 0.1, estimators = 1000, subsample = 1.0, criterion = Friedman MSE, tol = 0.0001, minimum samples split = 2, ccp alpha = 0.0, minimum samples leaf = 1, minimum weight fraction leaf = 0.0, maximum depth = 3, minimum impurity decrease = 0.0, validation fraction = 0.1

4.1. Performance under noisy and noise-free conditions

The features extracted from an analysis of the time–frequency domain are directly related to classification validity. Various noise conditions are applied to verify the effect of the proposed hybrid UWT-SVM under different noise levels. The k-nearest neighbors (kNN), SVM, DT, RF, Gradient Boosting Decision Tree (GBDT)'s test performance scores are given in Table 6. Improved SVM classifier gives successful results even in high noise PQD signals if the features obtained from UWT coefficients are used. The GBDT classifier also achieved substantial success in test data. If the properties obtained from the DWT coefficients are used, the GBDT classifier performance is higher than the SVM classifier. However, it shows lower performance than the classifiers used with UWT. When UWT is used instead of DWT in the signal decomposition process, DT shows higher accuracy classification performance. DT, which is frequently used in real-time applications, can also be used for high accuracy classification with UWT. However, since the classification accuracy obtained with DT is lower than the improved kernel SVM classifier, it was not preferred in this study.

The performance of the proposed method for each PQD event was investigated under different noise levels. To demonstrate the performance of the proposed event recognition method, a confusion matrix is used, which allows distinguishing correct events from misidentified events. The columns show the actual class and the rows correspond to the predicted class. The off-diagonal cells correspond to events that are incorrectly predicted, and diagonal cells correspond to events that are correctly predicted. The confusion matrix for nine classes using the proposed UWT and SVM-based method for different noise levels has shown in Table 7, Table 8, Table 9, and Table 10. The minimum accuracy of the proposed method for C9 disturbance is 97.7% under 25 dB high-level noise conditions. For other event classes, the accuracy of UWT-SVM is higher than 99% under all noise conditions.

The confusion matrix in Table 7 provides information on the recognition accuracy of each PQD signal for noise-free conditions. It can be seen that; the accuracy of proposed method is higher than 99.5% for each class. Also, the accuracy of the proposed method in distinguishing C2 (sag) and C4 (interruption) classes is lower than other PQDs. This is because that, the events which are very close to the limit value of the

Table 6
Test Data Performance accuracy (%) of ML-based multiclass classifiers.

	Classification accuracy (%)							
	Pure		25db		30db		40db	
Classifier	UWT	DWT	UWT	DWT	UWT	DWT	UWT	DWT
kNN	99.16	93.13	98.57	88.92	98.76	90.72	99.15	93.09
SVM	**99.85**	97.28	**99.32**	91.59	**99.50**	93.59	**99.76**	96.62
DT	98.76	95.43	97.95	85.36	98.11	87.86	98.41	92.50
RF	99.39	97.21	98.48	91.39	98.65	93.01	98.97	96.02
GBDT	99.59	**97.61**	99.17	**94.17**	99.29	**95.01**	99.50	**96.66**

Table 7
Confusion matrix for UWT-SVM classifier test results (pure signal)

	Predicted class								
Actual	C1	C2	C3	C4	C5	C6	C7	C8	C9
C1	586								
C2		587		3					
C3			630			1			
C4		3		608					
C5					619				
C6						593			
C7							626		
C8								616	
C9								1	612

Table 8
Confusion matrix for UWT-SVM classifier test results (40db)

	Predicted class								
Actual	C1	C2	C3	C4	C5	C6	C7	C8	C9
C1	645								
C2		553		5					
C3			596			1			
C4		4		594					
C5					639				
C6	1					623			
C7							599		
C8								622	
C9								2	591

Table 9
Confusion matrix for UWT-SVM classifier test results (30db)

	Predicted class								
Actual	C1	C2	C3	C4	C5	C6	C7	C8	C9
C1	589								
C2		605		3					
C3			619		2				
C4		5		615					
C5					576				
C6			1			584			
C7							596	5	
C8								595	
C9								11	596

distinguishing sag and interruption specified in the standards are also used in the test data.

The performance of the proposed method for each PQD event for 40 dB noise has shown in Table 8. It can be seen that; the proposed method shows the same accuracy in signals with 40 dB noise as in the noise-free condition.

The confusion matrix in Table 9 provides information about the recognition accuracy of each PQD signal under 30 dB high noise conditions. When the performance of the proposed method is examined, it is seen that the accuracy rate for C9 (notch) is relatively lower than for the other classes. Even in this case, the accuracy of the proposed method for the C9 event is 98.18%. Since the frequency components formed by the notch effect are very high, they cannot be defined with classical harmonic measuring devices. The proposed method performs notch detection with high accuracy. Also, samples for nearly all possible values of notch area and depth were included in the test data. The performance of the proposed method for each PQD event for 25 dB noise has shown in Table 10. It is seen that the features obtained with UWT, increase the classification accuracy even under very high noise conditions.

Table 10
Confusion matrix for UWT-SVM classifier test results (25db)

	Predicted class								
Actual	C1	C2	C3	C4	C5	C6	C7	C8	C9
C1	596								
C2		601		6					
C3			613		3				
C4		8		618					
C5					583				
C6			1			576			
C7							600	5	
C8								591	
C9								14	592

4.2. *Simulations of PQDs in microgrid*

The schematic view of the studied microgrid has shown in Fig. 8. The system consists of a PV plant, a double-fed induction generator (DFIG)-based wind turbine system (WTS), a delta/star connected step down two windings transformer, linear and nonlinear loads, capacitor bank, induction motor, and circuit breakers (CBs). The parameters of the studied system are shown in Table 11.

The interconnection of the renewable energy resources-based DGs to the microgrids could lead to PQ problems, degradation in system reliability, and other associated issues. The PQ problems occurring in the microgrids with the integration of renewable energy and DGs show similar features as there are in the conventional systems. On the other hand, some situations cause PQDs specific to DGs. Voltage regulation can become a challenge in the presence of DGs. Increased interconnection of single-phase renewable energy resources-based DGs in the distribution grid can affect the voltage profile. Again, environmental characteristics such as variation in wind speed and solar radiation largely influence the voltage signal in the PCC and may lead to voltage sag/voltage swell disturbances.

Some special operating conditions in DG will cause PQ problems, which is not the same as for the conventional power systems:

Voltage sag, interruption, and swell disturbances:

Depending on the fault location and DG operating mode conditions, a fault or functional problem may cause voltage sag, interruption, or swell. Voltage sag is described as a 10%–90% drop in the DG operating voltage for 1 to 9 cycles. Overloaded motors, switching on large loads, single phase-to-ground faults, and sudden startup of WTS cause voltage sag in DGs. Voltage sag signals are generated by a single phase-to-ground fault at PCC (0.4 kV bus) or end of the transmission line, several combinations of startup WTS generators, and switching on large

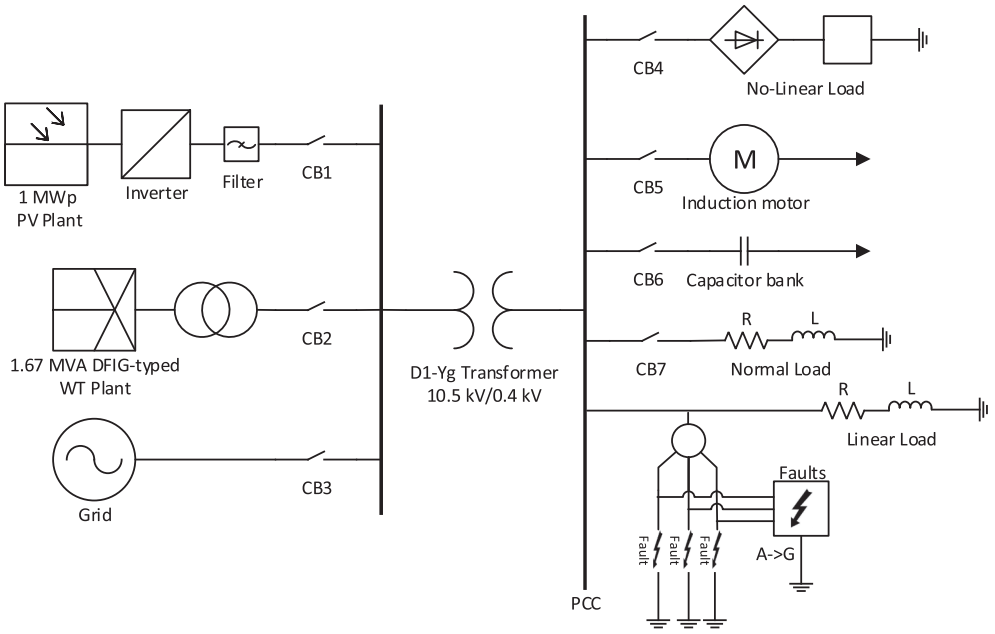

Fig. 8. The schematic view of the simulated microgrid.

Table 11
Parameters of the simulated test system.

	Parameters	Value
PV Plant	Maximum power (Pmax)	1 MWp
	Inverter output voltage	10.5 kV
	Inverter switching frequency	10 kHz
	Nominal frequency	50 Hz
DFIG-typed WTS	Apparent power (S_n)	1.67 MVA
	Active power	1.5 MW
	f	50 Hz
	Rs ≈Rr, Lr ≈ Ls	2.34 Ω, 0.0158H
	Max. power factor	0.37
Main Grid	Apparent power (S_n)	10 MVA
	3-phase short-circuit voltage (VA)	10 MV
	X/R ratio	7
Induction motor	Type	Squirrel cage
	Active power (P_n)	160 kW
	(n_n)	1487 rpm
Non-liner load	Active power	10 kW
	Inductive reactive power	1KVAr
	Controlled rectifier	6 pulse-Thyristor
Normal load	R-L Load	150 kVA
Transformer	Voltage level	10.5 kV /0.4 kV
	Winding Connection	$\Delta - Y$
	Rating Apparent power (S_n)	1 MVA
	R_{0pu},L_{0pu}	0.002, 0.08
Capacitor Bank	Reactive power	40 kVAr – 60 kVAr
	V_n	400 V

loads at PCC.

Voltage interruption disturbance defines a drop of more than 90% of the voltage amplitude for 1 to 9 cycles in DG. Double phase-to-ground faults and three-phase symmetrical faults cause voltage interruption depending on short circuit resistance in power systems. Besides, in DG structure, switching on large loads in island mode, CB tripping, and component failures may also cause interruption. In the studied DG system, voltage interruption disturbance signals are generated by adding double phase-to-ground faults and three-phase symmetrical faults at the PCC (0.4 kV bus). Several combinations of DG outputs and DG loads are used in the test set. Nominal voltage condition, voltage interruption, and voltage sag events waveform sample for the recorded test set are shown in Fig. 9.

The voltage swell event defines a rise of 10%–80% of the voltage amplitude in the DG., limited to a time interval of 1 to 9 cycles. Phase-to-phase faults, switching of the loads, and switching on large capacitor banks may cause voltage swell in the power system. Besides, the surge of WTS or PV generators may also cause voltage swell in DGs. In the studied microgrid, voltage swell disturbance signals are generated by adding phase-to-phase faults, switching large loads, and switching on large capacitor banks at PCC.

- **Impulsive and oscillatory transient, harmonics, flicker, and notches disturbances:**

The oscillatory transients, notches, flickers, and harmonics can be generated by nonlinear loads, significant short circuit faults, large capacitor banks, large load switching, and operation mode switching in DG applications.

In the studied DG system, oscillatory transient signals are generated by switching large loads and switching on a large capacitor bank at PCC. A non-linear load is fed through a six-pulse converter to generate the notch disturbances. Besides, impulsive transients are generated by developed lightning and electrostatic discharge block with MATLAB/Simulink. Furthermore, transformer energization causes harmonics in the simulated microgrid system. Several combinations of DG outputs and DG loads are used in the test set. Generated oscillatory transient and notches waveforms are shown in Fig. 10.

The detection result of the proposed UWT and SVM-based hybrid method is shown in Table 12. The proposed hybrid method is suitable to detect and classify PQDs caused by short circuit faults, switching of large loads, switching of large capacitor banks, presence of drive systems with nonlinear loads, and transformers energization in DG system-based microgrid.

4.3. Comparative analysis with existing methods

As shown in Table 13, the PQDs classification accuracy corresponding to the UWT and SVM-based algorithm is higher than all the other investigated methods. It can be observed that some techniques [8,23,32,33] have high accuracy. Still, they have no information about classification accuracy under low- high-level noise conditions.

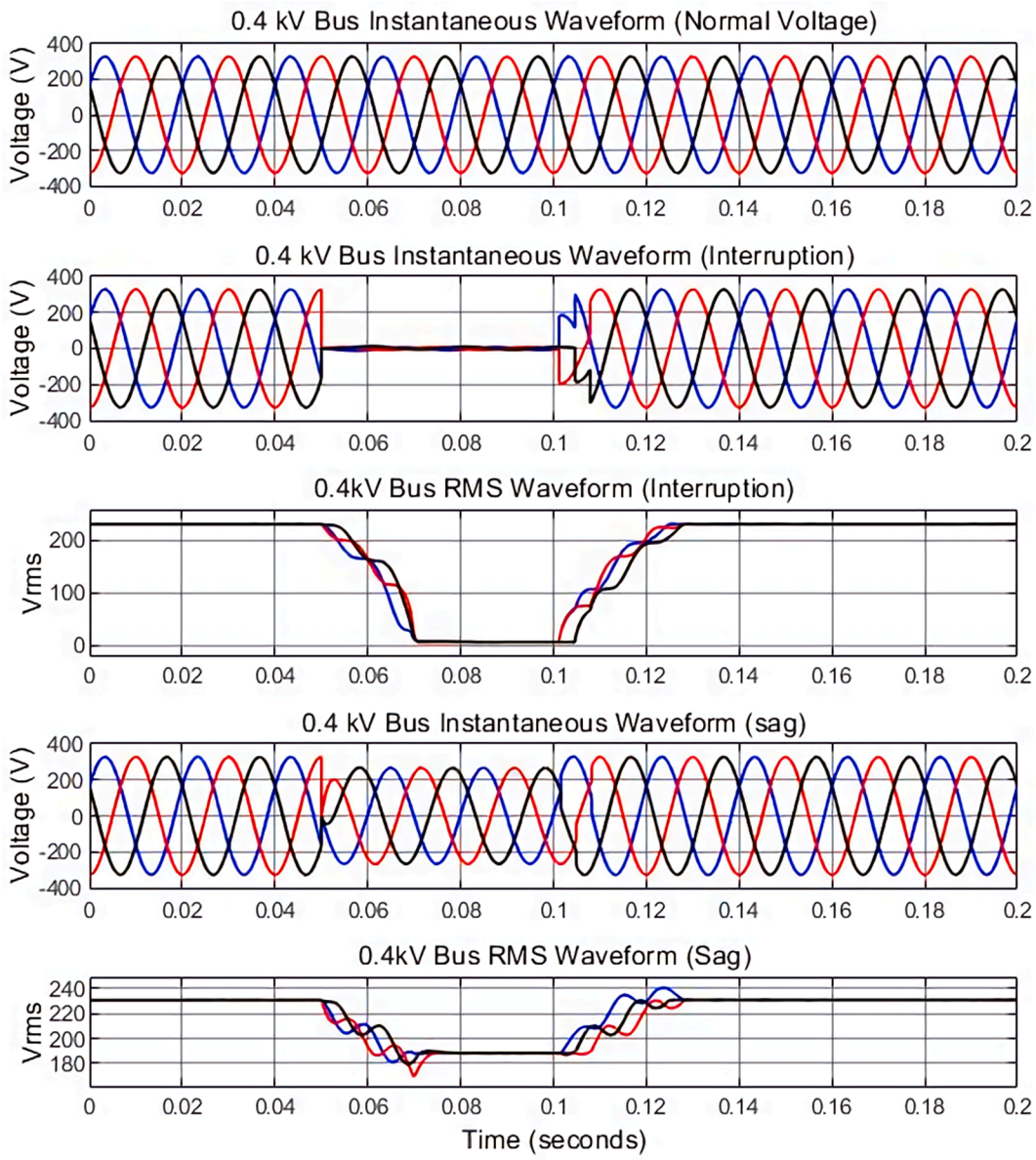

Fig. 9. PCC Instantaneous and effective voltage waveforms.

Ref. [8,34,35] utilize more features than other PQD classification methods. Using many features can increase classification performance, but it also increases the computational time.

The proposed method classification accuracy for PQDs under different noise levels and no-noise conditions is higher than the other methods except deep learning-based methods in references [33,39]. Ref. [33] uses 1D and 2D deep convolutional neural network (DCNN) with high complexity. Therefore, the proposed DCNN method is very difficult to use in real-time applications. A hybrid method using both the WVD and CNN is proposed in ref. [39]. Although the classification accuracy is very high in this method, it requires a large processing load because it uses both a signal analysis method and a complex classifier architecture.

The classification accuracy under the low and high-level noise conditions is 99.66% and 99.37%, respectively, for the proposed method. As shown in Table 13, WT is used in many studies [8,9,18,32,35], but it has many deficiencies, especially in the analysis of noisy signals. As the noise ratio in the signal increases, the reliability of the developed WT-based detection systems decreases. These drawbacks in the literature have been eliminated with the proposed UWT and SVM-based hybrid method.

4.4. Real data validation of PQDs in DG system

One hundred thirty groups of measured single-phase PQDs are used at the PCC in the experimental test system to validate the proposed method. The studied test system in the laboratory is shown in Fig. 11. The test system consists of A PV array, a single-phase inverter, and different loads in typical industrial applications. Sags, swells, transients, harmonics, flickers, and notches are generated by these loads, such as a parallel RL load, capacitor bank, single-phase induction machine, and variable speed drive a three-phase induction motor. Experimental setup composed of 1200 Wp PV array, Sunny boy 1300 Wp inverter, 1.1. kVA three-phase induction motor, 1 hp (746 W) single-phase induction motor, 40 mF capacitor bank, 50 Ω, and 63 mH RL load. The single-phase voltage signal information acquired by the voltage measurement card and data acquisition card at the PCC is transmitted to the LabVIEW software for processing. LA-55-P type sensor is used to obtain a PCC voltage signal in an electronic measurement card in real-time. MX USB-6221 DAQ card was used to acquire data from the test system. The sampling frequency is selected as 10 kHz. The voltage signal is acquired for 0.2 s, obtaining 2000 points. Typical industrial loads are connected

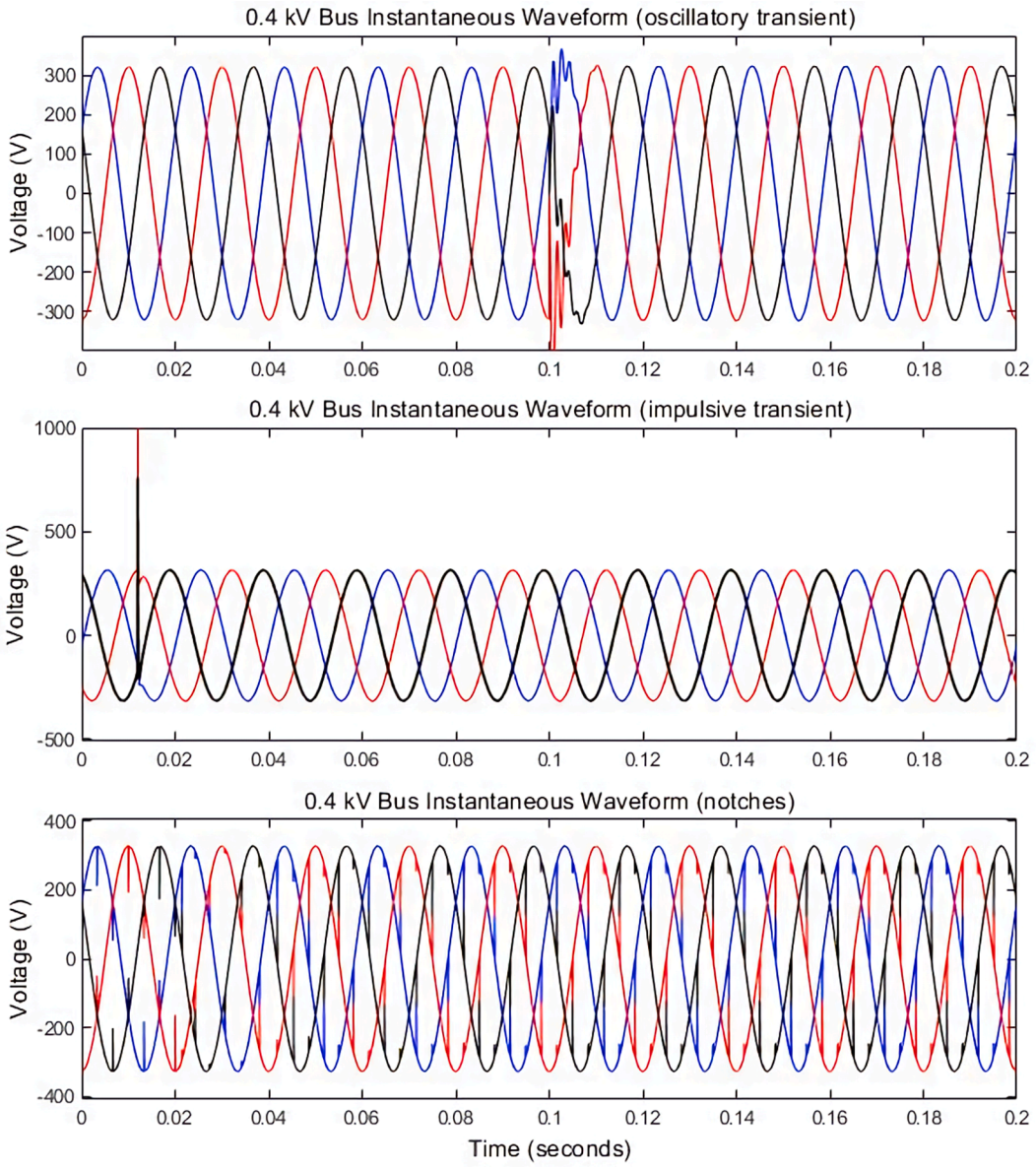

Fig. 10. PCC voltage waveforms caused by oscillatory transient, impulsive transient, and notches.

Table 12
UWT-SVM classifier test results of the simulation.

PQDs	Test Samples	Correction
Voltage Sag	20	20
Voltage Swell	20	20
Voltage Interruption	20	20
Harmonics	15	15
Flicker	3	3
Oscillatory transient	10	10
Impulsive transient	8	8
Notch	5	5

or disconnected to generate PQD signals.

The trained UWT-SVM model was used to identify the acquired PQD data. The real data results are shown in Table 14. The proposed hybrid method is suitable to detect and classify PQDs, and it is proved that the proposed method is more accurate in the classification of PQDs.

Table 13
Performance comparison of existing methods.

Method	Number of Class	Accuracy (%)		
		Pure	40 dB	30 dB
ST and APNN [7]	11	98.2	—	—
WPT and SVM [8]	8	99.66	—	—
DWT and PNN [9]	9	99.87	98.6	95.2
EWT and SVM [18]	9	97.22 (25–55 dB mixed data)		
DRST and SVM [19]	9	97.77 (20 dB data)		
ARTMAP and WT [32]	8	99.66	—	—
1D and 2D DCNN [33]	13	99.97	—	—
VMD and SVM [34]	9	99.66	—	99.33
QWT and SVM [35]	14	99.12	—	97.28
GDR and SVM [36]	10	94.2 (20–50 dB mixed data)		
ST and PNN [37]	9	99.26	99.13	98.63
CNN-LSTM [38]	6	84.76 (real data)		
WVD + CNN [39]	9	99.67 (10–40 dB mixed data)		
Proposed method	**9**	**99.85**	**99.76**	**99.50**

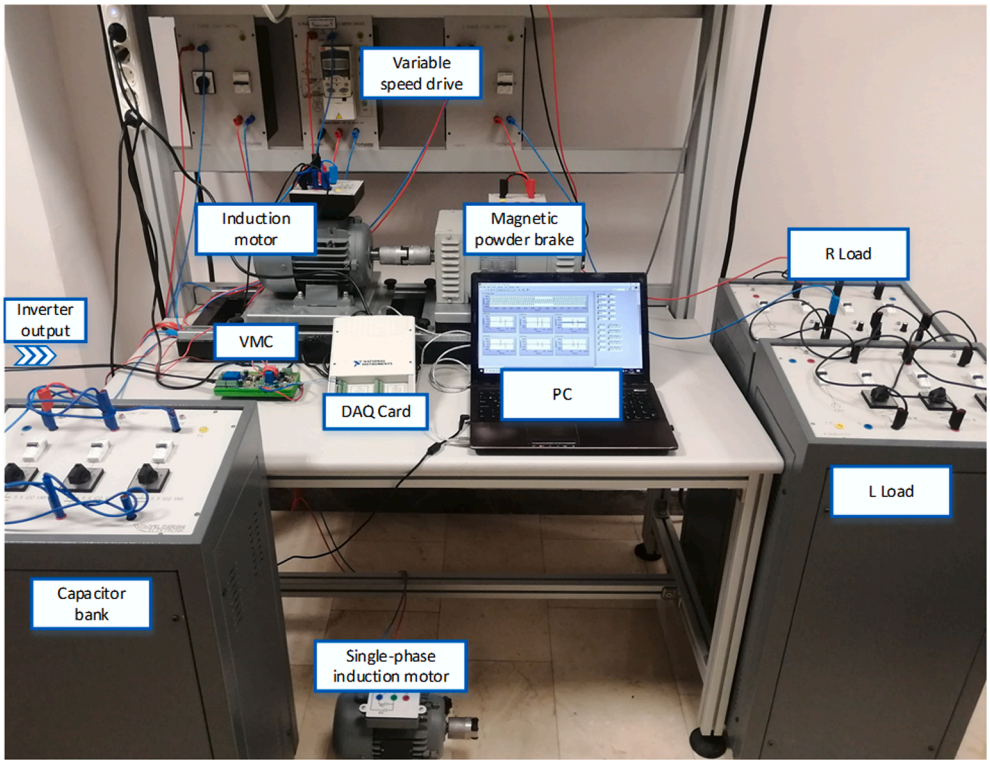

Fig. 11. Structure of the real-time test system.

Table 14
SVM classifiers test results of real data using DWT and UWT.

PQDs	Test Samples	Correction	
		UWT	DWT
Voltage Sag	35	34	29
Voltage Swell	35	34	30
Harmonics	15	15	15
Flicker	10	10	15
Transient	20	20	15
Notch	15	15	14

5. Conclusion

A new hybrid, UWT-based feature extraction method by using a kernel SVM is proposed for the classification of PQDs in DGs. For the first time in the literature, the UWT method with the "á trous" algorithm was used for feature extraction in PQD signals in microgrid and investigated with different classifiers. UWT-based decomposition improved the resolution of time–frequency analysis. The classifiers' performance, which is developed based on WT but has low performance under noise, has been dramatically improved with UWT. Furthermore, UWT decomposition has advantages in peak or valley detection and it obtains high-frequency resolution at high frequencies.

To assess the performance of the proposed scheme, different classifiers kNN, SVM DT, RF, and GBDT have been considered. The accuracy performance of all classifiers using UWT-obtained features is significantly higher than those using DWT-obtained features. In DT, which is frequently used in real-time applications, when UWT is used in the feature extraction process, the classification accuracy is 97.95% under 25 dB very high noise, while this rate is 85.36% when DWT is used. GBDT performance decreases usually caused by overfitting the noise in the signal. The performance of GBDT, which is the fastest algorithm in testing/prediction, decreases usually caused by overfitting the noise in the signal. With the UWT process, this disadvantage is eliminated, and a high degree of classification accuracy of 99.17% can be achieved. Thanks to the proposed method, the popularity of GBDT in the power system may increase.

The overall recognition test accuracy for the PQDs is 99.85% for the proposed UWT and SVM-based hybrid method. The classification accuracy under low-level noise and high-level noise conditions is 99.66% and 99.32%, respectively. It provides better performance than state-of-the-art PQD classification methods. As a result, it shows that using the proposed SVM &UWT-based hybrid method provides more reliability and easily presents usable results in the classification of PQDs in DG systems.

Acknowledgment

This work was supported in part by the Scientific Research Projects Unit of Bursa Technical University, Bursa, Turkey, under Grant numbers: 182N06 and 190Y018.

References

[1] Muscas C. Power quality monitoring in modern electric distribution systems. IEEE Instrum Meas Mag 2010;13(5):19–27. https://doi.org/10.1109/MIM.2010.5585070.
[2] Khetarpal P, Tripathi MM. A critical and comprehensive review on power quality disturbance detection and classification 2020;Vol. 28. https://doi.org/10.1016/j.suscom.2020.100417.
[3] Chawda, G. S., Shaik, A. G., Shaik, M., Padmanaban, S., Holm-Nielsen, J. B., Mahela, O. P., & Kaliannan, P. (2020). Comprehensive Review on Detection and Classification of Power Quality Disturbances in Utility Grid with Renewable Energy Penetration. In *IEEE Access* (Vol. 8, pp. 146807–146830). Institute of Electrical and Electronics Engineers Inc. https://doi.org/10.1109/ACCESS.2020.3014732.
[4] Gadanayak DA. Protection algorithms of microgrids with inverter interfaced distributed generation units—A review. In: Electric Power Systems Research, Vol. 192. Elsevier Ltd.; 2021. https://doi.org/10.1016/j.epsr.2020.106986.

[5] Wang S, Chen H. A novel deep learning method for the classification of power quality disturbances using deep convolutional neural network. Appl Energy 2019; 235:1126–40. https://doi.org/10.1016/j.apenergy.2018.09.160.

[6] Ray PK, Mohanty SR, Kishor N. Classification of power quality disturbances due to environmental characteristics in distributed generation system. IEEE Trans Sustainable Energy 2013;4(2):302–13. https://doi.org/10.1109/TSTE.2012.2224678.

[7] Lee CY, Shen YX. Optimal feature selection for power-quality disturbances classification. IEEE Trans Power Delivery 2011;26(4):2342–51. https://doi.org/10.1109/TPWRD.2011.2149547.

[8] Manimala K, Selvi K, Ahila R. Optimization techniques for improving power quality data mining using wavelet packet-based support vector machine. Neurocomputing 2012;77(1):36–47. https://doi.org/10.1016/j.neucom.2011.08.010.

[9] Khokhar S, Mohd Zin AA, Memon AP, Mokhtar AS. A new optimal feature selection algorithm for classification of power quality disturbances using discrete wavelet transform and probabilistic neural network. Measurement: Journal of the International Measurement Confederation 2017;95:246–59. https://doi.org/10.1016/j.measurement.2016.10.013.

[10] Latran MB, Teke A. A novel wavelet transform-based voltage sag/swell detection algorithm. Int J Electr Power Energy Syst 2015;71:131–9. https://doi.org/10.1016/j.ijepes.2015.02.040.

[11] Karegar HK, Sobhani B. Wavelet transform method for islanding detection of wind turbines. Renewable Energy 2012;38(1):94–106. https://doi.org/10.1016/j.renene.2011.07.002.

[12] Pinto SJ, Panda G. Wavelet technique-based islanding detection and improved repetitive current control for reliable operation of grid-connected PV systems. Int J Electr Power Energy Syst 2015;67:39–51. https://doi.org/10.1016/j.ijepes.2014.11.008.

[13] Andrade LCM, Oleskovicz M, Fernandes RAS. Adaptive threshold based on wavelet transform applied to the segmentation of single and combined power quality disturbances. Applied Soft Computing Journal 2016;38:967–77. https://doi.org/10.1016/j.asoc.2015.10.061.

[14] Yılmaz A, Bayrak G. A real-time UWT-based intelligent fault detection method for PV-based microgrids. Electr Power Syst Res 2019;177:105984. https://doi.org/10.1016/j.epsr.2019.105984.

[15] Starck, J. L., Donoho, D. L., & Elad, M. (2004). Redundant multiscale transforms and their application for morphological component separation. *Adv. Imaging Electron Phys.* (DAPNIA-2004-88).

[16] Silva KM, Souza BA, Brito NSD. Fault detection and classification in transmission lines based on wavelet transform and ANN. IEEE Trans Power Delivery 2006;21(4): 2058–63. https://doi.org/10.1109/TPWRD.2006.876659.

[17] Valtierra-Rodriguez M, de Jesus Romero-Troncoso R, Osornio-Rios RA, Garcia-Perez A. Detection and classification of single and combined power quality disturbances using neural networks. IEEE Trans Ind Electron 2014;61(5):2473–82. https://doi.org/10.1109/TIE.2013.2272276.

[18] Thirumala K, Pal S, Jain T, Umarikar AC. A classification method for multiple power quality disturbances using EWT-based adaptive filtering and multiclass SVM. Neurocomputing 2019;334:265–74. https://doi.org/10.1016/j.neucom.2019.01.038.

[19] Li J, Teng Z, Tang Q, Song J. Detection and Classification of Power Quality Disturbances Using Double Resolution S-Transform and DAG-SVMs. IEEE Trans Instrum Meas 2016;65(10):2302–12. https://doi.org/10.1109/TIM.2016.2578518.

[20] Igual R, Medrano C, Arcega FJ, Mantescu G. Integral mathematical model of power quality disturbances. In: Proceedings of International Conference on Harmonics and Quality of Power; 2018. https://doi.org/10.1109/ICHQP.2018.8378902.

[21] *IEEE Recommended Practices for Monitoring Electric Power Quality*; IEEE Std 1159-1995; IEEE-SASB Coordinating Committees: New York, NY, USA, 1995.

[22] Camarena-Martinez D, Valtierra-Rodriguez M, Perez-Ramirez CA, Amezquita-Sanchez JP, de Jesus Romero-Troncoso R, Garcia-Perez A. Novel Downsampling Empirical Mode Decomposition Approach for Power Quality Analysis. IEEE Trans Ind Electron 2016;63(4):2369–78. https://doi.org/10.1109/TIE.2015.2506619.

[23] Mishra S, Bhende CN, Panigrahi BK. Detection and classification of power quality disturbances using S-transform and probabilistic neural network. IEEE Trans Power Delivery 2008;23(1):280–7. https://doi.org/10.1109/TPWRD.2007.911125.

[24] Puliyadi Kubendran AK, Loganathan AK. Detection and classification of complex power quality disturbances using S-transform amplitude matrix-based decision tree for different noise levels. International Transactions on Electrical Energy Systems 2017;27(4):e2286. https://doi.org/10.1002/etep.v27.410.1002/etep.2286.

[25] Das S, Pradhan AK, Kedia A, Dalai S, Chatterjee B, Chakravorti S. Diagnosis of Power Quality Events Based on Detrended Fluctuation Analysis. IEEE Trans Ind Electron 2018;65(9):7322–31. https://doi.org/10.1109/TIE.2018.2795559.

[26] Narayanaswami R, Sundaresan D, Ranjan Prema V. The Mystery Curve: A Signal Processing Based Power Quality Disturbance Detection. IEEE Trans Ind Electron 2021;68(10):10078–86. https://doi.org/10.1109/TIE.2020.3026268.

[27] Shensa MJ. The Discrete Wavelet Transform: Wedding the a trous and Mallat Algorithms. IEEE Trans Signal Process 1992;40(10):2464–82. https://doi.org/10.1109/78.157290.

[28] Bayrak G, Yilmaz A. Signal processing-based automated fault detection methods for smart grids. Smart Technologies for Smart Cities 2020;57. https://doi.org/10.1007/978-3-030-39986-3_4.

[29] National Instruments, LabVIEW 2014 advanced signal processing toolkit manual (2014). Available Online: https://zone.ni.com/reference/en-XX/help/372656C-01/lvasptconcepts/wa_uwt/.

[30] Saini MK, Beniwal RK. Optimum fractionally delayed wavelet design for PQ event detection and classification. International Transactions on Electrical Energy Systems 2017;27(10):e2408. https://doi.org/10.1002/etep.v27.1010.1002/etep.2408.

[31] Tang Q, Qiu W, Zhou Y. Classification of Complex Power Quality Disturbances Using Optimized S-Transform and Kernel SVM. IEEE Trans Ind Electron 2020;67 (11):9715–23. https://doi.org/10.1109/TIE.4110.1109/TIE.2019.2952823.

[32] Decanini JGMS, Tonelli-Neto MS, Malange FCV, Minussi CR. Detection and classification of voltage disturbances using a Fuzzy-ARTMAP-wavelet network. Electr Power Syst Res 2011;81(12):2057–65. https://doi.org/10.1016/j.epsr.2011.07.018.

[33] Sindi H, Nour M, Rawa M, Öztürk Ş, Polat K. A novel hybrid deep learning approach including combination of 1D power signals and 2D signal images for power quality disturbance classification. Expert Syst Appl 2021;174:114785. https://doi.org/10.1016/j.eswa.2021.114785.

[34] Abdoos AA, Khorshidian Mianaei P, Rayatpanah Ghadikolaei M. Combined VMD-SVM-based feature selection method for classification of power quality events. Appl Soft Computing J 2016;38:637–46. https://doi.org/10.1016/j.asoc.2015.10.038.

[35] Thirumala K, Siva Prasad M, Jain T, Umarikar AC. Tunable-Q Wavelet Transform and Dual Multiclass SVM for Online Automatic Detection of Power Quality Disturbances. IEEE Trans Smart Grid 2018;9(4):3018–28. https://doi.org/10.1109/TSG.2016.2624313.

[36] Borrás MD, Bravo JC, Moñtano JC. Disturbance Ratio for Optimal Multi-Event Classification in Power Distribution Networks. IEEE Trans Ind Electron 2016;63(5): 3117–24. https://doi.org/10.1109/TIE.2016.2521615.

[37] Wang H, Wang P, Liu T. Power quality disturbance classification using the S-transform and probabilistic neural network. Energies 2017;10(1):107. https://doi.org/10.3390/en10010107.

[38] Garcia CI, Grasso F, Luchetta A, Piccirilli MC, Paolucci L, Talluri G. A comparison of power quality disturbance detection and classification methods using CNN, LSTM, and CNN-LSTM. Appl Sci (Switzerland) 2020;10(19):1–22. https://doi.org/10.3390/app10196755.

[39] Cai K, Cao W, Aarniovuori L, Pang H, Lin Y, Li G. Classification of Power Quality Disturbances Using Wigner-Ville Distribution and Deep Convolutional Neural Networks. IEEE Access 2019;7:119099–109. https://doi.org/10.1109/Access.628763910.1109/ACCESS.2019.2937193.